On the noninvasive optical monitoring and differentiation of methemoglobinemia and sulfhemoglobinemia

Gladimir V. G. Baranoski, Tenn F. Chen, Bradley W. Kimmel, Erik Miranda, and Daniel Yim
University of Waterloo, Natural Phenomena Simulation Group, School of Computer Science, 200 University Avenue West, Waterloo, Ontario, Canada N2L 3G1

Abstract. There are several pathologies whose study and diagnosis is impaired by a relatively small number of documented cases. A practical approach to overcome this obstacle and advance the research in this area consists in employing computer simulations to perform controlled *in silico* experiments. The results of these experiments, in turn, may be incorporated in the design of differential protocols for these pathologies. Accordingly, in this paper, we investigate the spectral responses of human skin affected by the presence of abnormal amounts of two dysfunctional hemoglobins, methemoglobin and sulfhemoglobin, which are associated with two life-threatening medical conditions, methemoglobinemia and sulfhemoglobinemia, respectively. We analyze the results of our *in silico* experiments and discuss their potential applications to the development of more effective noninvasive monitoring and differentiation procedures for these medical conditions. © *2012 Society of Photo-Optical Instrumentation Engineers (SPIE).* [DOI: 10.1117/1.JBO.17.9.097005]

1 Introduction

The spectral appearance of human skin is largely affected by pathological conditions that lead to changes in the way that light is normally attenuated within its different layers. In blood-perfused tissues, such as the skin papillary and reticular dermis, such changes are associated with variations in the concentration of blood-borne pigments, notably hemoglobin.[1]

Most of the oxygen carried by blood is reversibly bound to hemoglobin molecules stored in the erythrocytes (red blood cells). A hemoglobin molecule encapsulates four heme porphyrin rings,[2] each with a centrally localized iron atom. These iron atoms are capable of binding with oxygen when they are in a ferrous (Fe^{2+}) state. However, if an iron atom is oxidized (loses an electron) to a ferric (Fe^{3+}) state, it can no longer bind to oxygen.

The oxygenated and deoxygenated states of hemoglobin correspond to its two functional forms, namely oxyhemoglobin (O_2Hb) and deoxyhemoglobin (HHb). In addition to these normal forms of hemoglobins, other dysfunctional forms of hemoglobin that do not bind oxygen reversibly can also be present in the erythrocytes, namely carboxyhemoglobin (COHb), methemoglobin (MetHb), and sulfhemoglobin (SHb).[3,4]

In normal physiological states, only small traces (<2%) of COHb and MetHb are found in human blood,[46] while SHb is absent.[6,7] However, the presence of dysfunctional hemoglobins in human blood may increase during abnormal physiological states. In the case of MetHb and SHb, the focus of this study, such an increase is usually associated with two potentially fatal medical conditions, methemoglobinemia and sulfhemoglobinemia, respectively. While MetHb corresponds to a reversible form of oxidized hemoglobin, SHb corresponds to an irreversible (lasts the lifetime of the erythrocyte) form of oxidized hemoglobin resulting from the incorporation of a sulfur atom in its porphyrin ring.[6,7]

Methemoglobinemia is a life-threatening condition whose symptoms worsen as the MetHb level increases, with a high occurrence of mortality being observed at MetHb levels above 70%.[4] Although methemoglobinemia is most commonly caused by exposure to an oxidizing chemical reagent, including those used in healthcare settings,[8] it may also arise from genetic or idiopathic etiologies.[4] The therapy for mild cases of methemoglobinemia is focused on the removal of the provoking substance, oxygen administration, and observation, while severe cases are usually treated with the administration of methylene blue, an efficacious electron donor.[4]

Although sulfhemoglobinemia is a rare medical condition, it can be caused by commonly used over-the-counter medications (e.g., phenazopyridine), and it can lead to end-organ damage and death when SHb reaches high levels (above 60%).[7] In fact, most of the drugs and chemical agents that cause methemoglobinemia can also cause sulfhemoglobinemia.[7–9] Unlike methemoglobinemia, which is reversible with a known antidote, methylene blue, sulfhemoglobinemia cannot be reverted using a chemical agent. There is no specific treatment for sulfhemoglobinemia, and extreme cases need to be managed through blood transfusions, which themselves may pose risks to the patients.[7]

The visual differentiation of methemoglobinemia and sulfhemoglobinemia is a challenging task since both can result in an abnormal skin appearance (cyanosis), notably in the body extremities.[4,10] If a patient with sulfhemoglobinemia is wrongly diagnosed as having methemoglobinemia and treated with methylene blue, not only will the patient not respond to the

Address all correspondence to: Gladimir V. G. Baranoski, University of Waterloo, Natural Phenomena Simulation Group, School of Computer Science, 200 University Avenue West, Waterloo, Ontario, Canada N2L 3G1. Tel: 1-519-8884567; Fax: 1-519-8851208; E-mail: gvgbaran@curumin.math.uwaterloo.ca

treatment, but he or she may be also subjected to other health risks such as renal failure.[8] In addition, the visual monitoring of the patient's condition will be further impaired since cyanosis can be masked by the presence of methylene blue.[8] Hence, the early clinical differentiation between methemoglobinemia and sulfhemoglobinemia is essential for their effective monitoring and treatment.

Methemoglobinemia produces arterial blood that is chocolate brown in color.[8] Accordingly, a basic screening test for methemoglobinemia consists of visually inspecting the color of a blood sample. Although such a test can help to differentiate the presence of MetHb from HHb,[4] it may be ineffective to differentiate the presence of MetHB from SHb due to their similar spectral properties.[7] A logical step to attempt to differentiate between methemoglobinemia and sulfhemoglobinemia involves the use of optical measurement devices.

One laboratory device often employed in the diagnosis of blood-related conditions is the co-oximeter, a bench-top analyzer that accepts whole blood samples and uses four or more wavelengths of monochromatic light to spectroscopically differentiate the individual forms of hemoglobin in the sample.[4,9] However, available co-oximeters vary considerably, and SHb is often erroneously detected as MetHb, giving a false-positive result for methemoglobinemia.[7,9–11] Although more accurate and reliable results can be obtained through gas chromatography,[11] this procedure requires not only highly specialized equipment, but also a high degree of expertise.[7]

In the 1980s, the need for timely clinical information about blood oxygenation levels and the desire to minimize the inconvenience of extracting a blood sample and later analyze it in the lab led to the development of an alternative.[3,12] The search for noninvasive methods to differentiate methemoglobinemia and sulfhemoglobinemia is motivated by similar guidelines, with an extra difficulty being imposed by the small number of reported cases[7,8] and the scarcity of spectral data related to these conditions.[9]

In the last decades, computer simulations, or *in silico* experiments, are increasingly being employed by researchers to investigate and predict the behavior of complex biological processes, and to drive new experiments.[13] These *in silico* experiments can accelerate the hypothesis generation and validation cycles of biomedical research involving optical processes that cannot be fully studied through traditional laboratory procedures due to practical constraints. Among these constraints, one can highlight the difficulty to perform *in vivo* measurements and the relatively large number of biophysical variables that need to be controlled during the investigations. In the case of light and human tissue interaction processes, the information derived from *in silico* experiments not only contributes to broaden the current knowledge about these processes, but also has relevant biomedical applications such as the noninvasive assessment of tissue optical properties required for the diagnosis and treatment of diseases.[14,15]

The work presented in this paper follows the following approach. We employ a computational framework to simulate changes in cutaneous spectral reflectance due to the abnormal presence of MetHb and SHb in skin specimens with different levels of melanin pigmentation. These simulations were performed using a predictive spectral model of light interaction with human skin (BioSpec) whose algorithms and evaluation are fully described in the scientific literature.[16,17] The results of our *in silico* experiments indicate specific differences in

the spectral signatures of skin specimens subjected to methemoglobinemia and sulfhemoglobinemia. We believe that these differences, which have not been reported in the biomedical literature before, may have potential applications in the design of more effective noninvasive optical procedures for the monitoring and differentiation of these life-threatening conditions. To allow the full reproducibility of our findings, we made our *in silico* experimental framework and supporting biophysical data openly available online.[18]

2 Materials and Methods

2.1 *Biospec Model Overview*

For completeness, we outline the main characteristics of the BioSpec model[16,17] in this section. The BioSpec algorithmic design considers the stratification of human skin into four main layers: stratum corneum, epidermis, papillary dermis, and reticular dermis. Since the focus of this work is on the effects of dysfunctional hemoglobins on skin spectral responses, more details are provided with respect to the blood-perfused tissues (papillary and reticular dermis).

The BioSpec model employs ray optics techniques and Monte Carlo algorithms, which offer a flexible and yet rigorous approach to simulate the processes of light propagation (surface reflection, subsurface reflection, and transmission) and absorption within turbid multi-layered tissues.[14] Within the BioSpec simulation framework, light and skin interactions are described as a random walk process (that relies on the generation of random numbers ξ_j, for $j = 1, 2, \ldots$, uniformly distributed in the interval $[0, 1]$). In this random walk process, the transition probabilities are associated with Fresnel coefficients computed at each interface between the layers, and the termination probabilities are determined by the ray free path length.

Once a ray impinges a skin specimen at the air/stratum corneum interface, it can be reflected to the environment or refracted into the stratum corneum. In the former case, the BioSpec model computes the distribution of the reflected light taking into account the aspect ratio (or oblateness) of the skin surface folds. If the ray penetrates the skin specimen, then it can be reflected and refracted multiple times within the skin layers before it is either absorbed or propagated back to the environment. In the epidermis and stratum corneum, scattering is simulated using angular displacements measured by Bruls and van der Leun.[19]

Every ray entering one of the dermal layers is initially tested for Rayleigh scattering. If the test fails or the ray has already been bounced off one of the dermal interfaces, then the ray is randomized around the normal direction using a warping function based on a cosine distribution in which the polar perturbation angle, α_c, and the azimuthal perturbation angle, β_c, are given by

$$(\alpha_c, \beta_c) = [\arc \cos(\sqrt{\xi_1}), 2\pi\xi_2]. \tag{1}$$

To perform the Rayleigh scattering test, the spectral Rayleigh scattering coefficient, $\mu_{RS}(\lambda)$, is computed using the appropriate expression for Rayleigh scattering involving particles.[20] Next, a random number ξ_3 is generated. If $\xi_3 < 1 - \exp^{-\mu_{RS}(\lambda)}$, then the ray is scattered using an azimuthal perturbation angle, β_R, given by $2\pi\xi_4$, and a polar perturbation angle, α_R, obtained using the following rejection sampling algorithm based on the Rayleigh scattering phase function:[20]

$$\text{do} \quad \alpha_R = \pi\xi_5 \quad \chi = \frac{3}{2}\xi_6$$

$$\text{while} \left[\chi > \frac{3\sqrt{6}}{8}(1 + \cos^2 \alpha_R) \sin \alpha_R \right].$$

Once a ray has been scattered, it is probabilistically tested for absorption. This test consists of estimating the ray free path length using an expression based on Beer's law.[15] This estimation employs the total absorption coefficient, $\mu_{ai}(\lambda)$, of a given layer i, which, in turn, accounts for the extinction coefficient and the concentration of the pigments present in this layer such as the eumelanin and pheomelanin found in the epidermis. Accordingly, the ray free path length, $p(\lambda)$, is computed using the following expression:

$$p(\lambda) = -\frac{1}{\mu_{ai}(\lambda)} \ln(\xi_7) \cos\theta, \tag{2}$$

where θ corresponds to the angle between the ray and the specimen's normal. If $p(\lambda)$ is greater than the thickness of the layer, then the ray is propagated; otherwise it is absorbed.

For example, in the papillary dermis total absorption coefficient is given by

$$\mu_a = [\mu_{ao}(\lambda) + \mu_{ad}(\lambda) + \mu_{amh}(\lambda) + \mu_{ash}(\lambda) + \mu_{ach}(\lambda)$$
$$+ \mu_{abc}(\lambda) + \mu_{abil}(\lambda)]\vartheta_p + \mu_{a_{base}}(\lambda)(1 - \vartheta_p), \tag{3}$$

where $\mu_{ao}(\lambda)$, $\mu_{ad}(\lambda)$, $\mu_{amh}(\lambda)$, $\mu_{ash}(\lambda)$, $\mu_{ach}(\lambda)$, $\mu_{abc}(\lambda)$, and $\mu_{abil}(\lambda)$ correspond to absorption coefficients of oxyhemoglobin, deoxyhemoglobin, methemoglobin, sulfhemoglobin, carboxyhemoglobin, β-carotene, and bilirubin, respectively, ϑ_p is the volume fraction of the papillary dermis occupied by blood, and $\mu_{a_{base}}(\lambda)$ represents the baseline skin absorption coefficient. The absorption coefficient of a given pigment j is given by:

$$\mu_{a_j}(\lambda) = \log_e(10) \frac{\varepsilon_j(\lambda)}{c_j}, \tag{4}$$

where $\varepsilon_j(\lambda)$ and c_j correspond to its spectral extinction coefficient and concentration respectively. To compute the reticular dermis total absorption coefficient, the volume fraction ϑ_p is replaced by ϑ_r (volume fraction of the reticular dermis occupied by blood).

It is worth noting that due to the relatively low magnitude of the baseline skin absorption coefficient[21] with respect to the absorption coefficients of the pigments mentioned above, notably in the visible domain, its effects are usually assumed to be negligible in this spectral domain.[22] In this investigation, we employed the same assumption.

We remark that the BioSpec source code and supporting simulation data (e.g., extinction coefficients curves for pigments) are available for download[18] so that researchers can fully reproduce the simulations presented in this work. Alternatively, BioSpec can be run online via a model distribution framework[23] that enables researchers to access the model's webpage,[18] manipulate simulation parameters, such as experimental conditions (e.g., angle of incidence and spectral range) and skin characterization data (e.g., percentage of epidermis occupied by melanosomes and the concentration of various pigments in the skin tissues), and receive customized simulation results.

2.2 Biophysical Data and Investigation Procedures

The biophysical data used in our simulations of the skin spectral responses are provided in Table 1. The values assigned for these parameters were selected within valid ranges reported in biomedical references, which are also indicated in Table 1. The extinction coefficient curves for the pigments (chromophores) considered in our simulations are presented in Fig. 1, and they are also available for download.[18]

Although BioSpec provides bidirectional readings, directional-hemispherical quantities can be obtained by integrating the outgoing light (rays) with respect to the collection hemisphere.[40] The modeled directional-hemispherical reflectance curves presented in this work were obtained using a virtual spectrophotometer,[16] and considering an angle of incidence

Table 1 Biophysical parameters characterizing skin specimens under normal conditions.

Parameter	Value	Reference
Aspect ratio of skin surface folds	0.75	24, 25
Thickness of stratum corneum	0.001 cm	26
Thickness of epidermis	0.01 cm	26
Thickness of papillary dermis	0.01 cm	27
Thickness of reticular dermis	0.1 cm	27
Radius of collagen fibers	25 nm	28
Concentration of eumelanin in the melanosomes	80 g/L	29, 30
Concentration of pheomelanin in the melanosomes	5.2 g/L	31
Concentration β-carotene in the stratum corneum	2.1^{-4} g/L	32
Concentration β-carotene in the epidermis	2.1^{-4} g/L	32
Concentration β-carotene in the blood	7.0^{-5} g/L	32
Concentration of bilirubin in the blood	0.05 g/L	33
Concentration of oxy/deoxyhemoglobin in the blood	147 g/L	1
Ratio of oxy/deoxyhemoglobin	75%	12
Concentration of methemoglobin in the blood	1.5 g/L	4
Concentration of carboxyhemoglobin in the blood	1.5 g/L	5
Concentration of sulfhemoglobin in the blood	0 g/L	6
Refractive index of stratum corneum	1.55	34
Refractive index of epidermis	1.4	15
Refractive index of papillary dermis	1.36	35
Refractive index of reticular dermis	1.38	35
Refractive index of collagen fibers	1.5	30
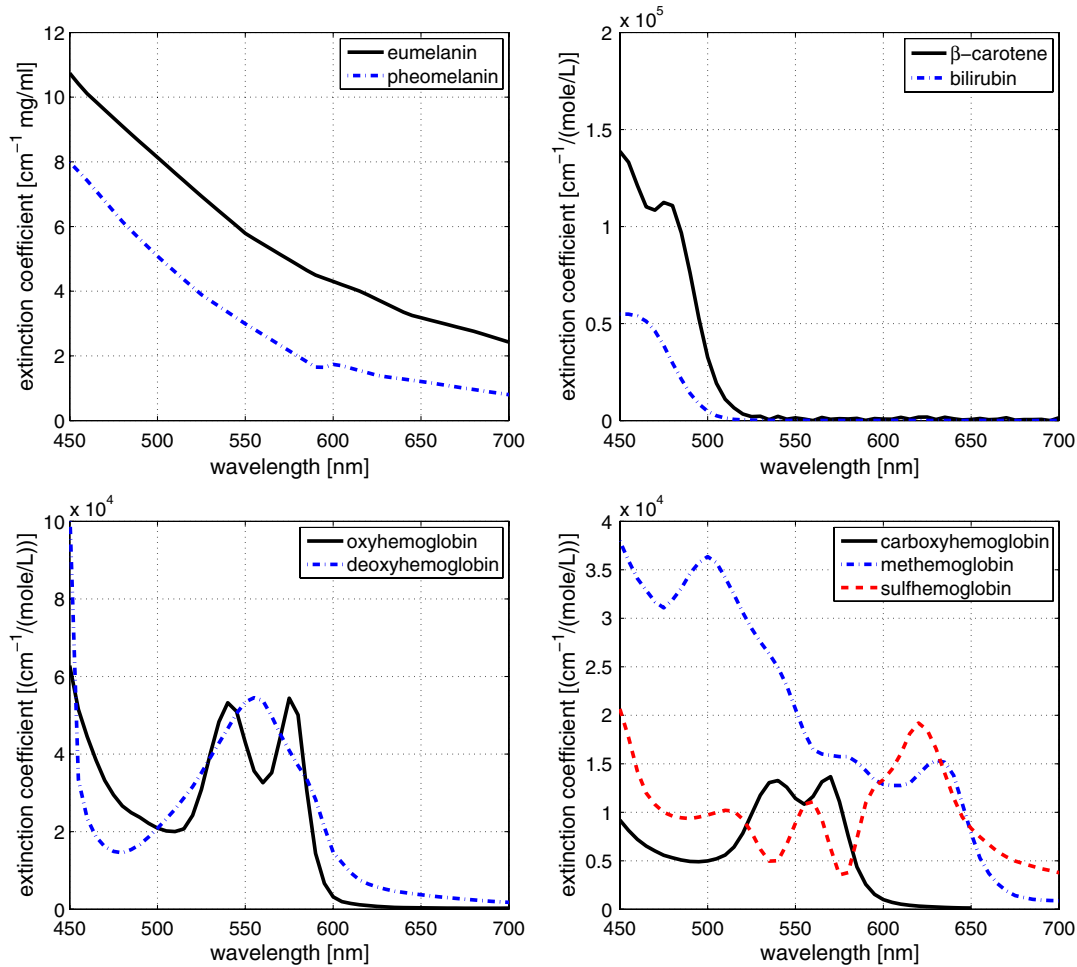
Fig. 1 Extinction curves of the pigments considered in our simulations. Top left: melanins.[35] Top right: β-carotene and bilirubin.[36] Bottom left: functional hemoglobins.[37] Bottom right: dysfunctional hemoglobins.[6,38,39]

measured with respect to the specimen's normal (zenith). These curves were computed with a spectral resolution of 5 nm and using 10^5 sample rays per data point.

In our *in silico* experiments, we considered skin specimens with different levels of pigmentation (Table 2), henceforth referred to as lightly pigmented (LP) and moderately pigmented (MP) specimens. These different levels of pigmentation are mostly associated with the percentage of epidermis occupied by melanosomes, which may vary from 1.3% for lightly pigmented specimens to 43% for darkly pigmented specimens.[30] Initially, we performed simulations considering the specimens

Table 2 Skin-related parameters employed in our simulations to characterize a lightly pigmented (LP) specimen and a moderately pigmented (MP) specimen.

Parameter	LP	MP
Percentage of epidermis occupied by melanosomes	1.6	3.6
Percentage papillary dermis occupied by blood	0.8	0.6
Percentage of reticular dermis occupied by blood	0.8	0.6

under normal conditions (Table 1). Although the presence of small traces (≈1%) of MetHb and COHb have a negligible impact on the spectral responses of healthy skin specimens, we have accounted for them in these simulations for consistency with the biomedical literature. We then compared the resulting modeled curves for the LP and MP specimens with measured curves provided by Vrhel et al.[41] These measurements were performed on the side of each subject's face, and they were made available in a spectra database at the North Carolina State University (NCSU spectral files 113 and 82, respectively). The pigmentation parameters used to generate the modeled curves (Table 2) were selected based on the skin type description of the actual specimens provided in the NCSU spectra database and the corresponding ranges for these parameters provided in the literature.[30] Both sets of modeled and measured curves were obtained considering the same angle of incidence (45 deg). Figure 2 also depicts computer-generated images illustrating the spectral appearance of the LP and MP specimens characterized by the parameters provided in Tables 1 and 2.

As depicted in Fig. 2, the simulations considering normal conditions resulted in a close agreement between the modeled and measured curves. Accordingly, we employed these modeled curves for specimens under normal conditions as the control (baseline) curves for our *in silico* experiments involving abnormal fractions of methemoglobin and sulfhemoglobin, i.e., we employed the same values for the simulation parameters
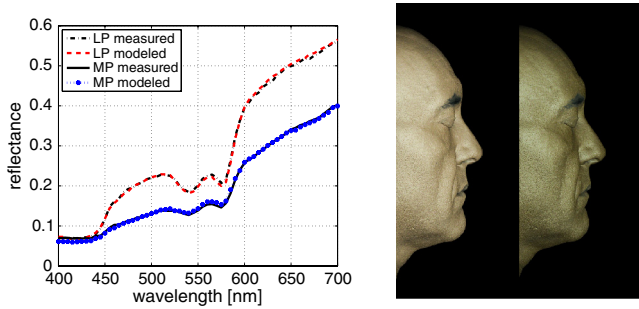
Fig. 2 Control (baseline) data used in our simulations. Left: comparisons of modeled spectral curves obtained using BioSpec with measured curves provided by Vrhel et al.[42] for lightly pigmented (LP) and moderately pigmented (MP) specimens. Right: computer-generated images illustrating the appearance of lightly pigmented (left) and moderately pigmented (right) specimens characterized by the parameters provided in Tables 1 and 2. These images were rendered using a path tracer algorithm[16] and skin spectral responses provided by the BioSpec model (head polygonal mesh courtesy of XYZ RGB Inc.).

(Table 1), with the exception of the hemoglobin-related parameters. More specifically, we decreased the concentration of the functional hemoglobins as we increased the fractions of MetHb and SHb with respect to the total amount of hemoglobin.

3 Results and Discussion

Comparisons of modeled spectral curves obtained considering different MetHb and SHb fractions are presented in Fig. 3. As the presence of these dysfunctional hemoglobins increases, the resulting reflectance curves, henceforth referred to as dysfunctional curves to facilitate the discussion, deviate from the control curves associated with normal conditions, with more pronounced deviations being observed for SHb curves. Furthermore, these deviations are also more noticeable for the lightly pigmented specimen since the presence of more melanin in the moderately pigmented specimen reduces the impact of the dysfunctional hemoglobins on the light absorption by these specimens. Feiner et al.[43] reported a similar masking effect of melanin on the detection of functional hemoglobins through pulse oximetry.

As it can be observed in Fig. 3, the MetHb and SHb dysfunctional curves deviate from the control curves in a similar qualitative manner for most parts of the visible spectrum. Note that the control and dysfunctional curves present an intersection at ≈593 nm, close to the isosbestic point of SHb and MetHB at ≈598 nm (Fig. 1). In the region from ≈525 to ≈593 nm, the dysfunctional curves show a decrease with respect to the control curves, while, in the region from ≈593 to ≈695 nm, they show an increase with respect to the control curves.

However, one can also observe some distinct behaviors for the dysfunctional curves. For example, the reflectance values associated with the MetHb curves tend to remain constant at ≈700 nm, while the reflectance values associated with the SHb curves show a noticeable decrease at this wavelength. In addition, from ≈475 to ≈525 nm, the MetHb curves show a decrease with respect to the control curves, while the SHb curves show an increase. A closer observation of the reflectance values at 500 nm, the approximated midpoint of this region, reveals a monotonic increase associated with increasing SHb levels (Table 3) and monotonic decrease associated with decreasing MetHb levels (Table 4).

To extend the scope of our observations, we selected a different angle of incidence, 0 deg, and repeated the simulations. The same quantitative and qualitative trends observed in the modeled curves obtained for an angle of incidence of 45 deg were observed in the modeled curves obtained for 0 deg (Fig. 4). In particular, the reflectance values at 500 nm also showed a monotonic increase with respect to increasing SHb levels (Table 5), and a monotonic decrease with respect to increasing MetHb levels (Table 6).

As mentioned before, the cyanotic effects of methemoglobinemia and sulfhemoglobinemia are more prominent in the body extremities,[4,10] such as the fingers, characterized by dermal tissues occupying a larger volume of blood.[3] Hence, to further extend our scope of observations, we repeated our *in silico* experiments using the parameters provided in Table 2, with the exception of the volume fraction of the reticular and papillary dermis occupied by blood, which we set to 5% for both specimens according to data provided in the biomedical literature.[3,30] The resulting spectral curves considering angles of incidence equal to 45 and 0 deg are presented in Figs. 5 and 6, respectively. Again, the same quantitative and qualitative trends were observed in the region from ≈475 to ≈525 nm, with the reflectance values at 500 nm showing a monotonic increase with respect to increasing SHb levels (Tables 7 and 8), and a monotonic decrease with respect to decreasing MetHb levels (Tables 9 and 10).

It is worth noting that actual spectral reflectance values are measured using devices such as spectrophotometers, which may be subjected to uncertainties. A high-precision device will have an uncertainty of ±0.001 or 0.1%.[44] A low-precision device may have an uncertainty close to 1%.[44,45] To assess the consistency of our observations with respect to these random fluctuations, we performed a set of simulations considering the presence of random noise (1%) in the biophysical parameters. The resulting spectral curves obtained considering an angle of incidence of 0 deg and 5% of the dermal tissues occupied by blood are presented in Fig. 7. As it can be observed by comparing these curves with the curves presented in Fig. 6 and by comparing the spectral values given in Tables 11 and 12 with the spectral values given in Tables 8 and 10, respectively, the trends remained the same.

The visual inspection of the MHb and SHb dysfunctional curves presented in Figs. 5 and 6 also indicates that these curves tend to have opposite slopes in the region from ≈600 to ≈630 nm. This trend is consistent with the distinct shapes of the MetHb and SHb extinction coefficient curves (Fig. 1) in this region. To investigate this trend more closely, we considered MetHb and SHb fractions from 10% to 70% (in increments of 10%), and computed the second derivative of the corresponding dysfunctional curves at 615 nm employing the following three-point central difference formula:[45]

$$y''(615) = \frac{\rho(600) - 2\rho(615) + \rho(630)}{225}, \qquad (5)$$

where $\rho(600)$, $\rho(615)$, and $\rho(630)$ correspond to reflectance values at 600, 615, and 630 nm, respectively.

As it can be observed in Table 13, the second derivative at 615 nm has a negative sign for the MetHb curves, and a positive sign for SHb curves, with the exception of the 10% SHb curves. This inconsistency at the 10% SHb level may be attributed to the dominant melanin masking effects. However, it is important to
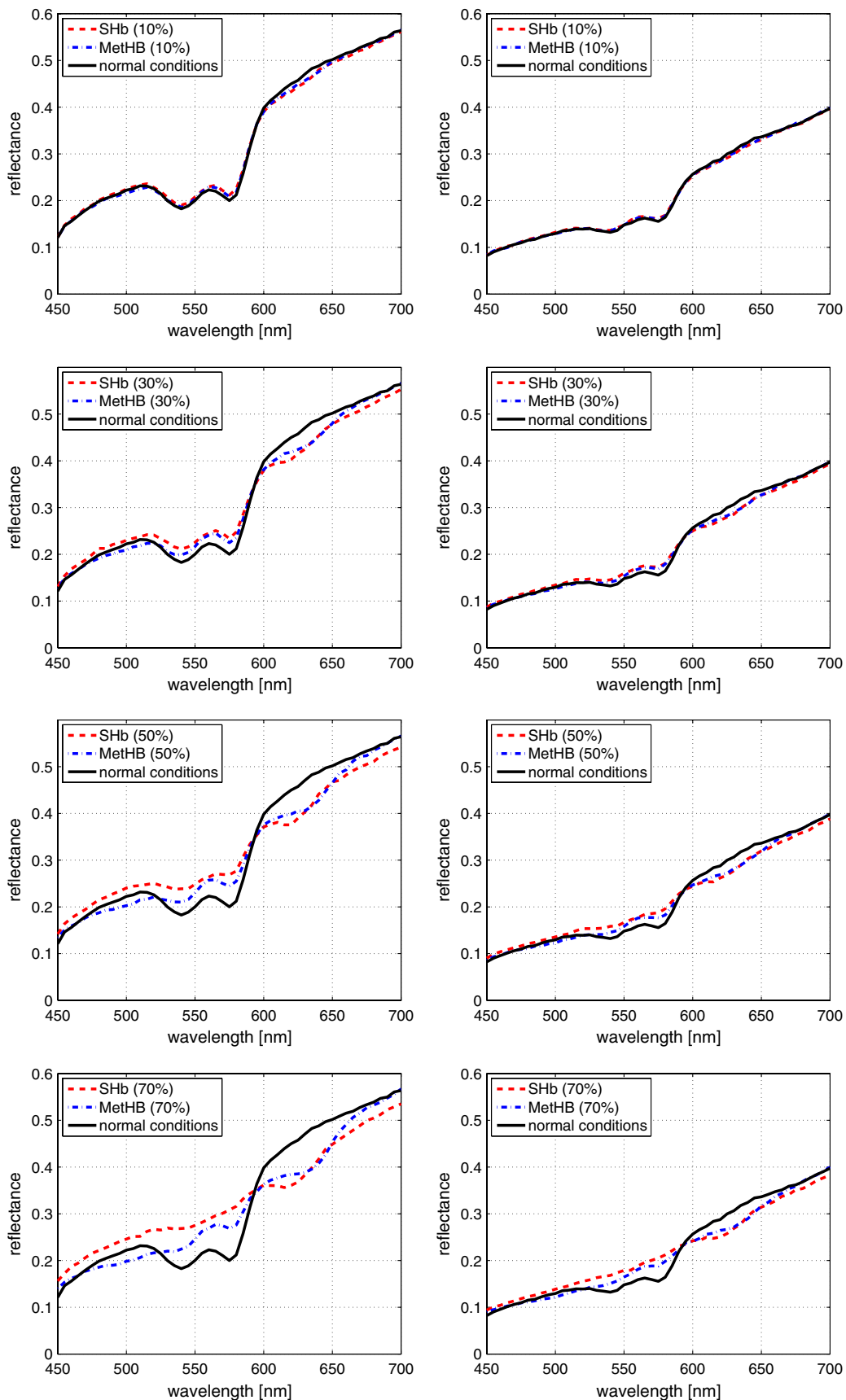
Fig. 3 Comparisons of modeled skin reflectance curves obtained considering an angle of incidence equal to 45 deg and different fractions of sulfhemoglobin (SHb) and methemoglobin (MHb). Left: lightly pigmented (LP) specimen. Right: moderately pigmented (MP) specimen.
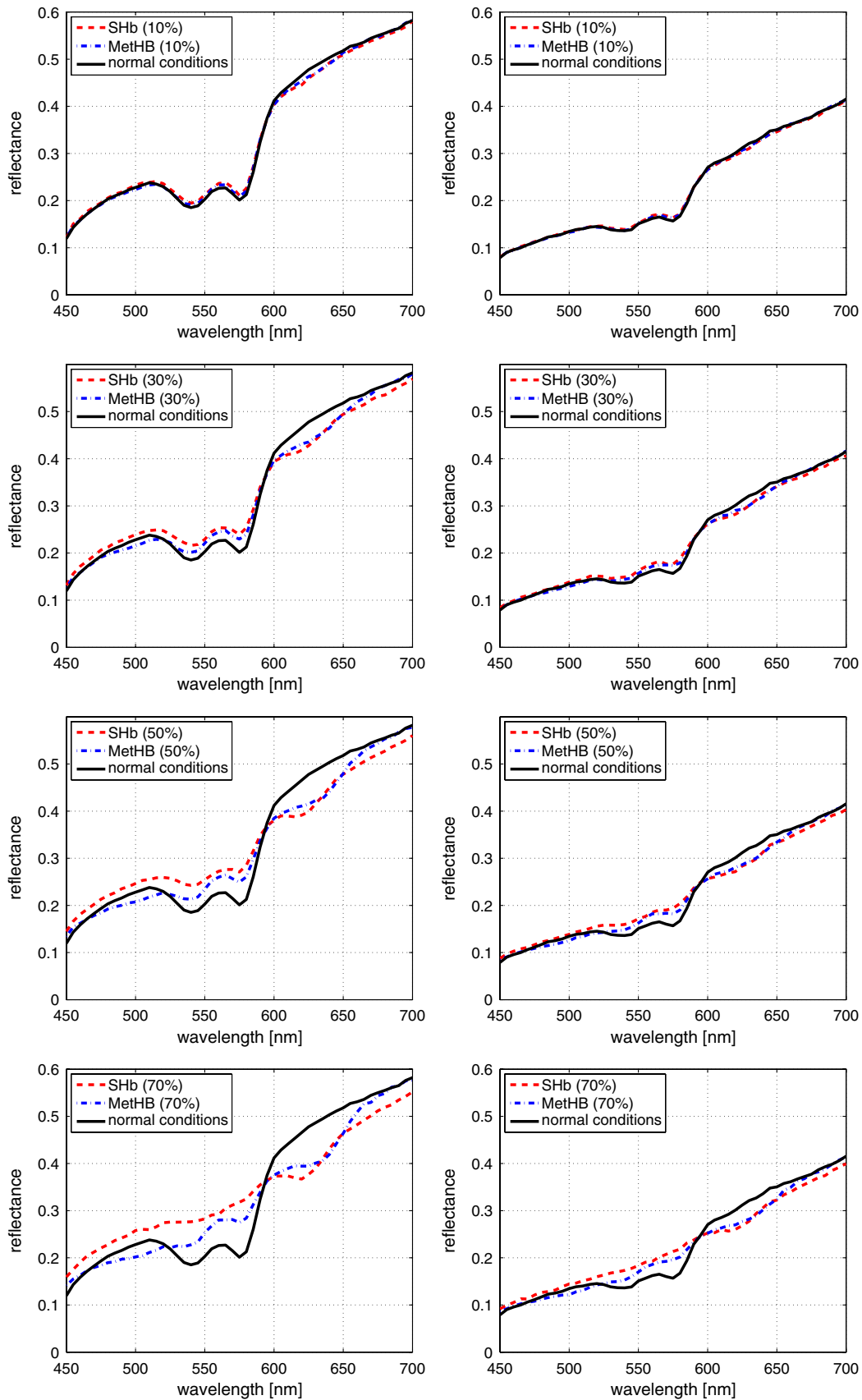
Fig. 4 Comparisons of modeled skin reflectance curves obtained considering an angle of incidence equal to 0 deg and different fractions of sulfhemoglobin (SHb) and methemoglobin (MHb). Left: lightly pigmented (LP) specimen. Right: moderately pigmented (MP) specimen.
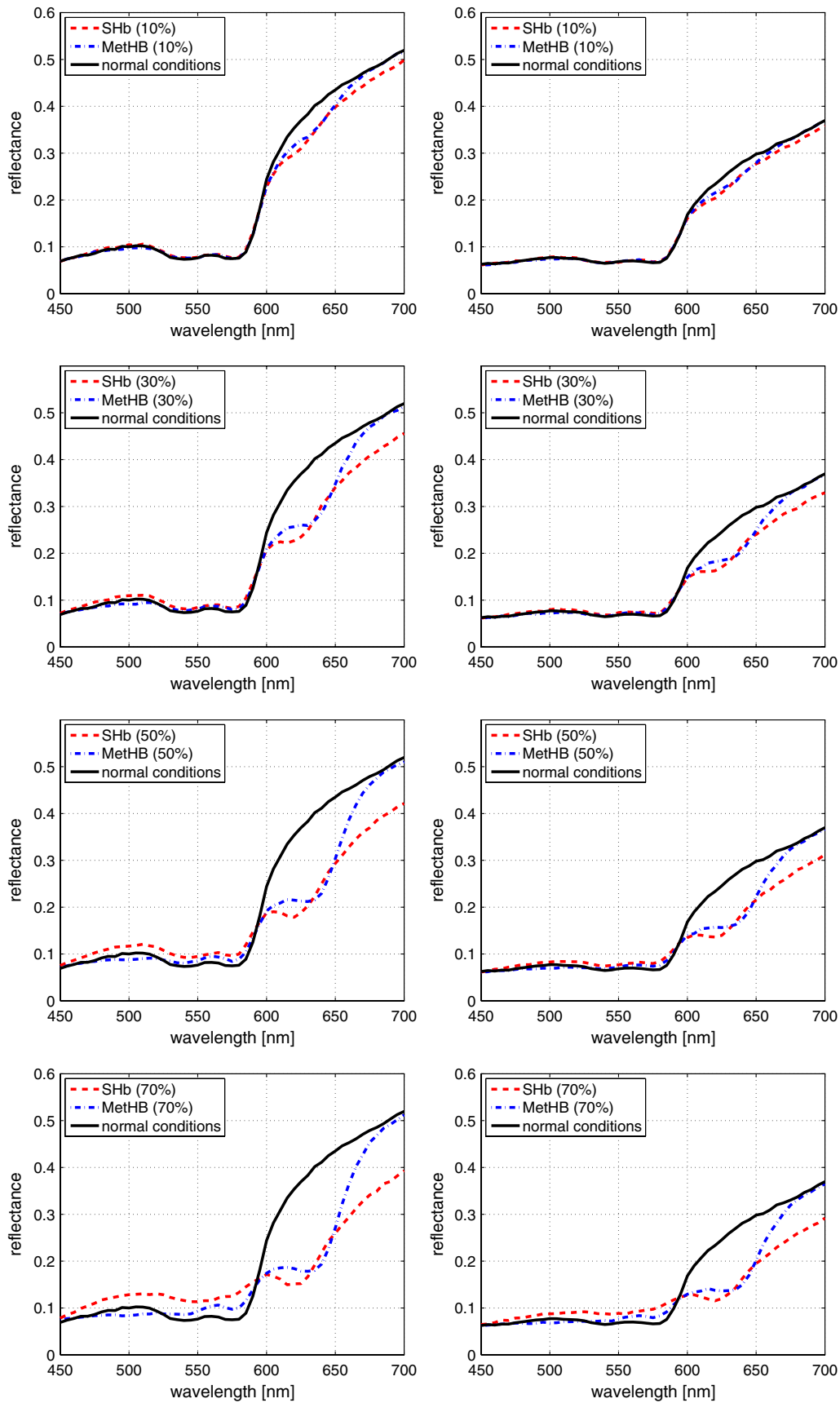
Fig. 5 Comparisons of modeled skin reflectance curves obtained considering an angle of incidence equal to 45 deg, 5% of the dermal tissues occupied by blood, and different fractions of sulfhemoglobin (SHb) and methemoglobin (MHb). Left: lightly pigmented (LP) specimen. Right: moderately pigmented (MP) specimen.

Fig. 6 Comparisons of modeled skin reflectance curves obtained considering an angle of incidence equal to 0 deg, 5% of the dermal tissues occupied by blood, and different fractions of sulfhemoglobin (SHb) and methemoglobin (MHb). Left: lightly pigmented (LP) specimen. Right: moderately pigmented (MP) specimen.
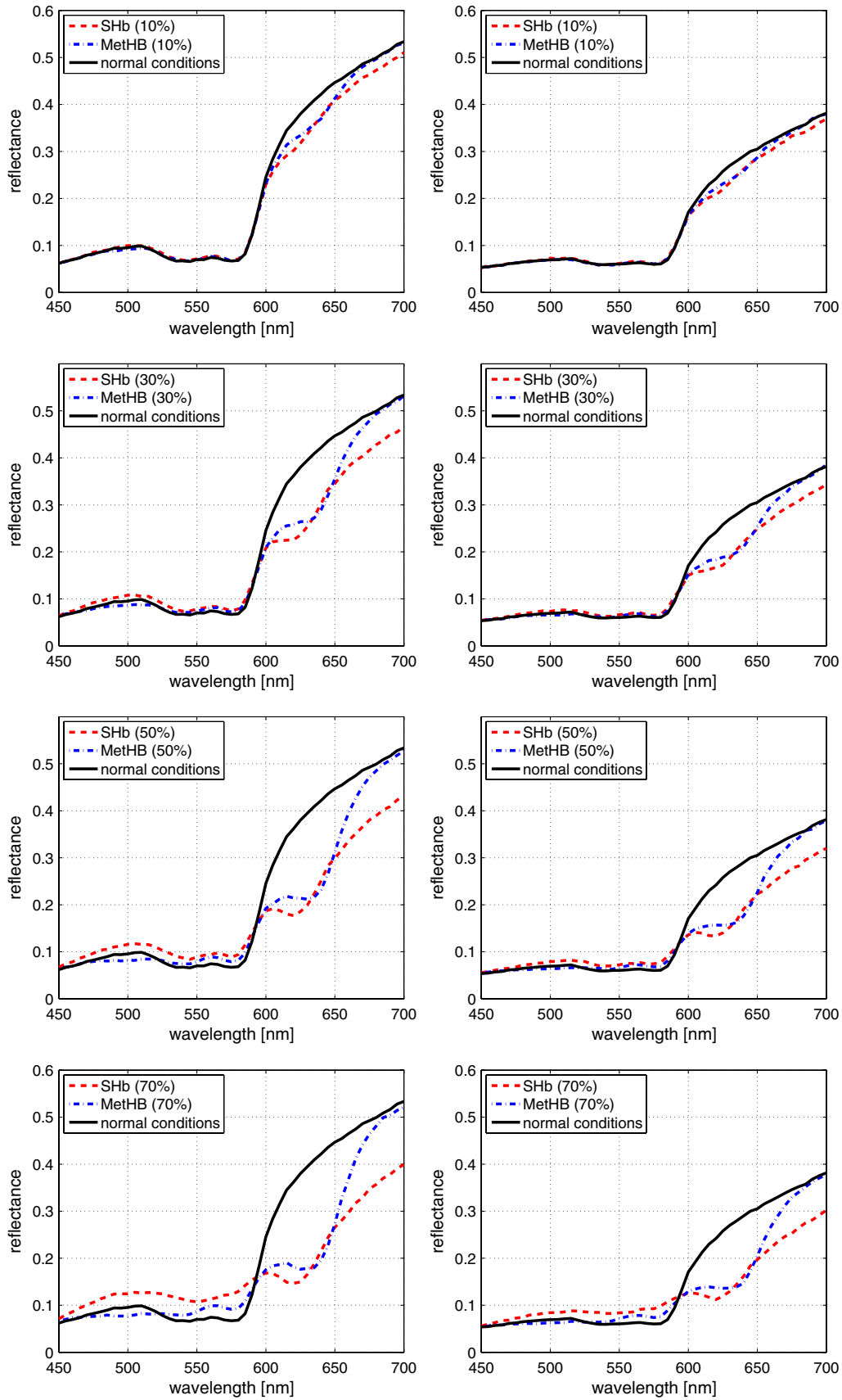
Table 3 Reflectance values at 500 nm extracted from the modeled spectral curves obtained considering an angle of incidence of 45 deg and different fractions of sulfhemoglobin (SHb) in the lightly pigmented (LP) specimen and in the moderately pigmented (MP) specimen.

	10%	30%	50%	70%
LP	0.2250	0.2299	0.2405	0.2459
MP	0.1324	0.1341	0.1357	0.1388

Table 4 Reflectance values at 500 nm extracted from the modeled spectral curves obtained considering an angle of incidence of 45 deg and different fractions of methemoglobin (MetHb) in the lightly pigmented (LP) specimen and in the moderately pigmented (MP) specimen.

	10%	30%	50%	70%
LP	0.2159	0.2088	0.2026	0.1985
MP	0.1292	0.1263	0.1227	0.1216

Table 5 Reflectance values at 500 nm extracted from the modeled spectral curves obtained considering an angle of incidence of 0 deg and different fractions of sulfhemoglobin (SHb) in the lightly pigmented (LP) specimen and in the moderately pigmented (MP) specimen.

	10%	30%	50%	70%
LP	0.2329	0.2391	0.2464	0.2579
MP	0.1337	0.1383	0.1386	0.1388

Table 6 Reflectance values at 500 nm extracted from the modeled spectral curves obtained considering an angle of incidence of 0 deg and different fractions of methemoglobin (MetHb) in the lightly pigmented (LP) specimen and in the moderately pigmented (MP) specimen.

	10%	30%	50%	70%
LP	0.2235	0.2157	0.2074	0.2018
MP	0.1328	0.1291	0.1250	0.1217

Table 7 Reflectance values at 500 nm extracted from the modeled spectral curves obtained considering an angle of incidence of 45 deg, 5% of the dermal tissues occupied by blood and different fractions of sulfhemoglobin (SHb) in the lightly pigmented (LP) specimen and in the moderately pigmented (MP) specimen.

	10%	30%	50%	70%
LP	0.1046	0.1096	0.1168	0.1285
MP	0.0780	0.0796	0.0828	0.0874

Table 8 Reflectance values at 500 nm extracted from the modeled spectral curves obtained considering an angle of incidence of 0 deg, 5% of the dermal tissues occupied by blood and different fractions of sulfhemoglobin (SHb) in the lightly pigmented (LP) specimen and in the moderately pigmented (MP) specimen.

	10%	30%	50%	70%
LP	0.0998	0.1080	0.1160	0.1243
MP	0.0731	0.0736	0.0792	0.0843

Table 9 Reflectance values at 500 nm extracted from the modeled spectral curves obtained considering an angle of incidence of 45 deg, 5% of the dermal tissues occupied by blood and different fractions of methemoglobin (MetHb) in the lightly pigmented specimen (LP) and in the moderately pigmented (MP) specimen.

	10%	30%	50%	70%
LP	0.0976	0.0915	0.0876	0.0839
MP	0.0738	0.0718	0.0693	0.0682

Table 10 Reflectance values at 500 nm extracted from the modeled spectral curves obtained considering an angle of incidence of 0 deg, 5% of the dermal tissues occupied by blood and different fractions of methemoglobin (MetHb) in the lightly pigmented specimen (LP) and in the moderately pigmented (MP) specimen.

|	10%	30%	50%	70%
LP	0.0921	0.0866	0.0831	0.0771
MP	0.0689	0.0652	0.0640	0.0622

highlight that the sign results are consistent for larger fractions of MetHb and SHb.

To assess whether the use of a higher order second derivative formula could lead to more consistent results for low ($\leq$10%) SHb fractions, we also performed the sign computations using the following five-point central difference formula:[46]

$$y''(615)$$
$$= \frac{-\rho(600) + 16\rho(607.5) - 30\rho(615) + 16\rho(622.5) - \rho(630)}{675},$$

(6)

where $\rho(600)$, $\rho(607.5)$, $\rho(615)$, $\rho(622.5)$, and $\rho(630)$ correspond to reflectance values at 600, 607.5, 615, 622.5, and 630 nm, respectively. The sign results obtained using this formula completely matched the sign results presented in Table 13, which indicates that a higher accuracy-to-cost ratio in these sign computations can be obtained using a three-point central difference formula for the second derivative at 615 nm.

Current procedures for the effective differentiation of methemoglobinemia and sulfhemoglobimenia rely on "wet" laboratory procedures.[4,7] Ideally, one would like to be able to accurately differentiate and monitor these life-threatening
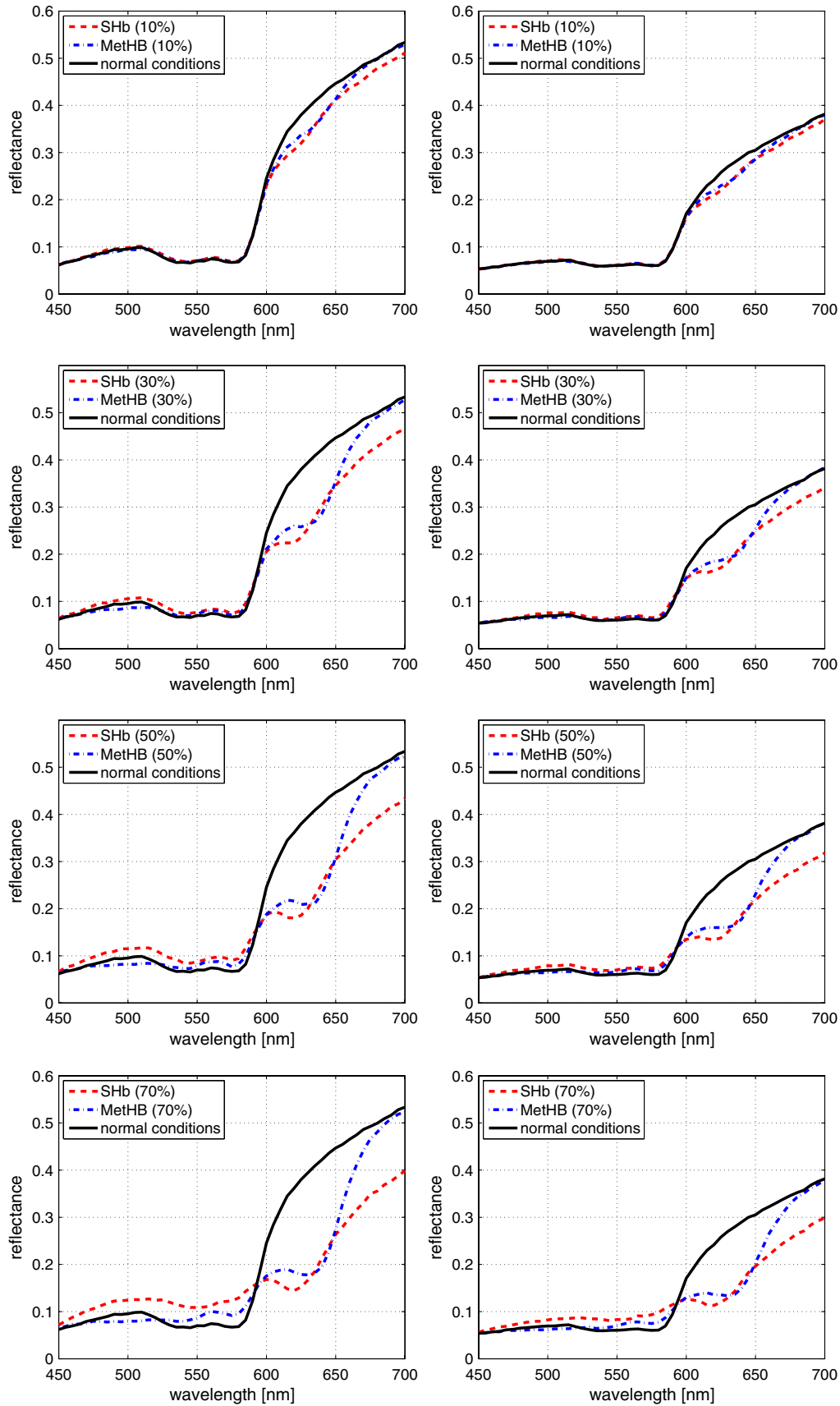
Fig. 7 Comparisons of modeled skin reflectance curves obtained considering the presence of random noise in the biophysical parameters, an angle of incidence equal to 0 deg, 5% of the dermal tissues occupied by blood, and different fractions of sulfhemoglobin (SHb) and methemoglobin (MHb). Left: lightly pigmented (LP) specimen. Right: moderately pigmented (MP) specimen.

Table 11 Reflectance values at 500 nm extracted from the modeled spectral curves obtained considering the presence of random noise in the biophysical parameters, an angle of incidence of 0 deg, 5% of the dermal tissues occupied by blood and different fractions of sulfhemoglobin (SHb) in the lightly pigmented (LP) specimen and in the moderately pigmented (MP) specimen.

	10%	30%	50%	70%
LP	0.0984	0.1058	0.1150	0.1243
MP	0.0691	0.0759	0.0790	0.0824

Table 12 Reflectance values at 500 nm extracted from the modeled spectral curves obtained considering the presence of random noise in the biophysical parameters, an angle of incidence of 0 deg, 5% of the dermal tissues occupied by blood and different fractions of methemoglobin (MetHb) in the lightly pigmented specimen (LP) and in the moderately pigmented (MP) specimen.

	10%	30%	50%	70%
LP	0.0938	0.0870	0.0822	0.0798
MP	0.0693	0.0665	0.0642	0.0613

conditions using noninvasive optical procedures. The results of our *in silico* experiments indicating that abnormal amounts of SHb and MetHb may result in distinct reflectance behaviors around 500 and 700 nm suggest that such an approach may be feasible. Our experiments also demonstrate that the melanin pigmentation level can significantly affect the detection of these spectral changes. In particular, our experiments indicate that reflectance differences are more noticeable for lightly pigmented specimens at 500 nm, and at 700 nm for moderately pigmented specimens. Hence, enhanced optical monitoring procedures for methemoglobinemia and sulfhemoglobimenia may need to consider

multiple measurement points to cope with different levels of melanin pigmentation.

Finally, our *in silico* experiments involving a larger amount of blood in the dermal tissues (a characteristic of body extremities) suggest that a noninvasive optical differentiation between methemoglobinemia and sulfhemoglobinemia can be carried out by taking reflectance measurements at 600, 615, and 630 nm on body extremities, and using these values to numerically determine the sign of the second derivative at 615 nm. We remark that standard pulse oximetry measurements are normally performed on a body location, such as a finger in adult patients, characterized by a relatively large blood content.[3,12] As indicated by our simulations, the outcomes of such a differentiation procedure are likely to be consistent for MetHb and SHb fractions at or above 20%, which are associated with more serious states of these medical conditions. Hence, the probability of false-negative screening results for increasingly severe cases of sulfhemoglobinemia and false-positive screening results for increasingly severe cases of methemoglobinemia tend to be null.

Although *in situ* experiments are required to assess the full applicability of our findings, we believe that they provide a sound basis for future investigations in this area. To allow the full reproduction and extension of our *in silico* experiments, we made the simulation framework and data employed in this work openly available for download.[18] Hence, researchers can either download an offline version of the BioSpec model and perform the simulations on their own computers, or run the simulations through our online system.[23] In the latter case, it may take approximately 25 s (on a dual 6-core 2.66-GHz Intel Xeon machine with 24 Gb of RAM) to obtain a spectral reflectance curve such as those presented in this work.

4 Conclusions

Methemoglobinemia and sulfhemoglobinemia are serious medical conditions that may lead to end-organ damage and death. Currently, the design of accurate noninvasive differentiation and monitoring protocols for these conditions is impaired by the relatively small number of cases reported in the biomedical literature. More specifically, the lack of *in situ* measured spectral data for human skin specimens affected by these conditions and

Table 13 Second derivative signs of the modeled dysfunctional curves at 615 nm. These curves were obtained considering 5% of the dermal tissues occupied by blood, two angles of incidence (45 and 0 deg), and different fractions of methemoglobin (MetHb) and sulfhemoglobin (SHb) in the lightly pigmented (LP) specimen and in the moderately pigmented (MP) specimen.

| | MetHb | | | | SHb | | | |
| | LP | | MP | | LP | | MP | |
	45 deg	0 deg	45 deg	0 deg	45 deg	0 deg	45 deg	0 deg
10%	−	−	−	−	−	−	−	−
20%	−	−	−	−	+	+	+	+
30%	−	−	−	−	+	+	+	+
40%	−	−	−	−	+	+	+	+
50%	−	−	−	−	+	+	+	+
60%	−	−	−	−	+	+	+	+
70%	−	−	−	−	+	+	+	+

the large number of variables involved in the light attenuation processes by these specimens precludes a detailed assessment of the effects of methemoglobin and sulfhemoglobin on human skin reflectance.

In this work, we have employed an *in silico* experimental approach to overcome these obstacles and perform the first detailed spectral investigation of methemoglobin and sulfhemoglobin effects on human skin reflectance. Using a predictive light transport model for human skin and sound biophysical data, we were able to perform controlled *in silico* experiments involving changes in the spectral signature of skin specimens affected by the presence of abnormal amounts of the dysfunctional hemoglobins in the dermal tissues. These experiments allowed us to identify specific reflectance trends that may be effectively applied to the noninvasive optical monitoring and differentiation of methemoglobinemia and sulfhemoglobinemia.

As future work, we plan to extend our investigation to the near-infrared domain. We also intend to take into account light sieve effects caused by other blood-related medical conditions such as anemia.

Acknowledgments

References

1. A. N. Yaroslavsky et al., "Optics of blood," in *Handbook of Optical Biomedical Diagnostics*, V. V. Tuchin, Ed., SPIE Press, Bellingham, WA (2002).
2. J. D. Spikes, "Photodynamic reactions in photomedicine," in *The Science of Photomedicine*, J. D. Regan and J. A. Parrish, Eds., pp. 113–144, Plenum Press, New York (1982).
3. R. Flewelling, "Noninvasive optical monitoring," in *The Biomedical Engineering Handbook*, J. D. Bronzino, Ed., pp. 1346–1356, IEEE Press, Boca Raton, Florida (1995).
4. S. Haymond et al., "Laboratory assessment of oxygenation in methemoglobinemia," *Clin. Chem.* **51**(2), 434–444 (2005).
5. A. J. Cunnington et al., "Carboxyhemoglobin levels in Kenyan children with plasmodium falciparum malaria," *Am. J. Trop. Med. Hyg.* **71**(1), 43–47 (2004).
6. I. H. Yarynovska and A. I. Bilyi, "Absorption spectra of sulfhemoglobin derivatives of human blood," *Proc. SPIE* **6094**, 60940G (2006).
7. L. Gharahbaghian, B. Massoudian, and G. DiMassa, "Methemoglobinemia and sulfhemoglobinemia in two pediatric patients after ingestion of hydroxylamine sulfate," *West. J. Emerg. Med.* **10**(3), 197–201 (2009).
8. E. Wolak et al., "Methemoglobinemia in critically ill burned patients," *Am. J. Respir. Crit. Care Med.* **14**(2), 104–108 (2005).
9. J. Lee et al., "Noninvasive *in vivo* monitoring of methemoglobin formation and reduction with broadband diffuse optical spectroscopy," *J. Appl. Physiol.* **100**(2), 615–622 (2006).
10. A. S. Gopalachar, V. L. Bowie, and P. Bharadwaj, "Phenazopyridine-induced sulfhemoglobinemia," *Ann. Pharmacother.* **39**(6), 1128–1130 (2005).
11. K. A. Nelson and M. A. Hosteler, "An infant with methoglobinemia," *Hosp. Phys.* **39**(2), 31–38, 62 (2003).
12. P. A. Öberg, "Optical sensors in medical care," *Sensors Update* **13**(1), 201–232 (2003).
13. B. D. Ventura et al., "From *in vivo* to *in silico* biology and back," *Nature* **443**(7111), 527–533 (2006).
14. L. Wang, S. L. Jacques, and L. Zheng, "MCML—Monte Carlo modelling of light transport in multi-layered tissues," *Comput. Methods Programs Biomed.* **47**(2), 131–146 (1995).
15. V. V. Tuchin, *Tissue Optics Light Scattering Methods and Instruments for Medical Diagnosis*, SPIE Press, Bellingham, WA (2007).
16. G. V. G. Baranoski and A. Krishnaswamy, *Light and Skin Interactions: Simulations for Computer Graphics Applications*, Morgan Kaufmann, Burlington, MA (2010).
17. A. Krishnaswamy and G. V. G. Baranoski, "A biophysically-based spectral model of light interaction with human skin," *Comput. Graph. Forum* **23**(3), 331–340 (2004).
18. NPSG (Natural Phenomena Simulation Group, University of Waterloo, Canada), "Run BioSpec online," (2011), http://www.npsg.uwaterloo.ca/models/biospec.php.
19. W. A. G. Bruls and J. C. van der Leun, "Forward scattering properties of human epidermal layers," *Photochem. Photobiol.* **40**(2), 231–242 (1984).
20. E. J. McCartney, *Optics of the Atmosphere: Scattering by Molecules and Particles*, John Wiley & Sons, New York (1976).
21. I. S. Saidi, "Transcutaneous optical measurement of hyperbilirubinemia in neonates," PhD Thesis, Rice University, Houston, TX (1994).
22. E. Angelopoulou, "Understanding the color of human skin," *Proc. SPIE* **4299**, 243–251 (2001).
23. G. V. G. Baranoski et al., "Rapid dissemination of light transport models on the web," *IEEE Comput. Graph. Appl.* **32**(3), 10–15 (2012).
24. P. S. Talreja et al., "Visualization of the lipid barrier and measurement of lipid pathlength in human stratum corneum," *AAPS PharmSci.* **3**(2), 1–9 (2001).
25 N. Thalmann et al., "A computational skin model: fold and wrinkle formation," *IEEE T. Inf. Technol. B* **6**(4), 317–323 (2002).
26. T. Gambichler et al., "Epidermal thickness assessed by optical coherence tomography and routine histology: preliminary results of method comparison," *J. Eur. Acad. Dermatol. Venereol.* **20**(7), 791–795 (2006).
27. P. Agache, "Main skin physical constants," in *Measuring the Skin*, P. Agache and P. Humbert, Eds., pp. 747–757, Springer-Verlag, Berlin (2004).
28. S. Li, "Biologic biomaterials: tissue-derived biomaterials (collagen)," in *Biomaterials Principles and Applications*, J. Park and J. Bronzano, Eds., pp. 117–139, CRC Press, Boca Raton, Florida (2003).
29. N. Kollias and A. Baqer, "On the assessment of melanin in human skin in vivo," *Photochem. Photobiol.* **43**(1), 49–54 (1986).
30. S. L. Jacques, "Origins of tissue optical properties in the UVA visible and NIR regions," *OSA Tops. Adv. Opt. Imaging Photon Migration* **2**, 364–369 (1996).
31. A. Hennessy et al., "Eumelanin and pheomelanin concentrations in human epidermis before and after UVB irradiation," *Pigment Cell Res.* **18**(3), 220–223 (2005).
32. R. Lee et al., "The detection of carotenoid pigments in human skin," *J. Invest. Dermatol.* **64**(3), 175–177 (1975).
33. C. R. Martin and J. P. Cloherty, "Neonatal hyperbilirubinemia," in *Manual of Neonatal Care*, J. P. Cloherty, E. C. Eichenwald, and A. R. Stark, Eds., pp. 181–212, Wolters Kluwer, Philadelphia (2008).
34. B. L. Diffey, "A mathematical model for ultraviolet optics in skin," *Phys. Med. Biol.* **28**(6), 647–657 (1983).
35. S. L. Jacques, C. A. Alter, and S. A. Prahl, "Angular dependence of HeNe laser light scattering by human dermis," *Lasers Life Sci.* **1**(4), 309–333 (1987).
36. S. L. Jacques, "Optical absorption of melanin," Oregon Medical Laser Center (2001), http://omlc.ogi.edu/spectra/melanin/index.html.
37. S. Prahl, "PhotochemCAD spectra by category," Oregon Medical Laser Center (2001), http://omlc.ogi.edu/spectra/PhotochemCAD/index.html.
38. S. Prahl, "Optical absorption of hemoglobin," Oregon Medical Laser Center (1999), http://omlc.ogi.edu/spectra/hemoglobin/index.html.
39. L. Randeberg et al., "Methemoglobin formation during laser induced photothermolysis of vascular skin lesions," *Laser. Surg. Med.* **34**(5), 414–419 (2004).
40. F. E. Nicodemus et al., "Geometrical considerations and nomenclature for reflectance" in *Physics-Based Vision Principles and Practice:*

Radiometry, L. B. Wolf, S. A. Shafer, and G. E. Healey, Eds., pp. 94–145, Jones and Bartlett Publishers, Washington, DC (1992).

41. M. J. Vrhel, R. Gershon, and L. S. Iwan, "Measurement and analysis of object reflectance spectra," *Color Res. Appl.* **19**(1), 4–9 (1994).

42. O. Siggaard-Andersen, B. Norgaard-Pedersen, and J. Rem, "Hemoglobin pigments spectrophotometric determination of oxy-, carboxy-, met-, and sulfhemoglobin in capillary blood," *Clinica Chimica Acta* **72**(1), 85–100 (1972).

43. J. R. Feiner, J. W. Severinghaus, and P. E. Bickler, "Dark skin decreases the accuracy of pulse oximeters at low oxygen saturation: the effects of oximeter probe type and gender," *Anesth. Analg.* **105**(6), S18–S23 (2007).

44. D. Judd and G. Wyszecki, *Color in Business, Science and Industry*, John Wiley & Sons, New York (1975).

45. G. A. Zerlaut and T. E. Anderson, "Multiple-integrating sphere spectrophotometer for measuring absolute spectral reflectance and transmittance," *Appl. Optics* **20**(21), 3797–3804 (1981).

46. C. F. Gerald and P. O. Wheatley, *Applied Numerical Analysis*, Addison-Wesley, Reading, MA (1999).